PAPER

Distinction between Mn(III) and Mn(II) by using a colorimetric chemosensor in aqueous solution†

Seul Ah Lee, Jae Jun Lee, Ga Rim You, Ye Won Choi and Cheal Kim*

A new colorimetric chemosensor for Mn(III) and Mn(II) was developed by combination of 2-(aminomethyl) aniline and 4-(diethylamino)-2-hydroxybenzaldehyde. This sensor **1** exhibited an obvious color change from pale yellow to reddish brown in the presence of Mn^{3+} in aqueous solution (buffer/CH_3CN = 7 : 3), which was reversible with the addition of EDTA. Moreover, **1** could be used to detect and quantify Mn^{3+} in water samples, and as a practical, visible colorimetric test kits for Mn^{3+}. Moreover, **1** could detect Mn^{2+} *via* the formation of **1**–Mn^{3+} complex with longer reaction time. The resulting different reaction time of Mn(III) and Mn(II) with **1** was used to differentiate between Mn(III) and Mn(II). Finally, the sensing ability of **1** for Mn^{3+} was supported by theoretical calculations.

1. Introduction

Selective and sensitive detection of trace metal ions has great significance both biologically and environmentally.[1–3] Hence, several analytical methods, including X-ray photoelectron spectroscopy (XPS), inductively coupled plasma atomic emission and mass spectroscopy (ICP-AES, ICP-MS) have been widely used for the detection of various metals even at a very low concentration.[4] However, these methods are relatively expensive, difficult to be applied and time-consuming. As an alternative to these expensive methods, a number of various chemosensors have been reported to date.[5–10] Among them, colorimetric chemosensor is a powerful tool for the detection and quantification of metal ions and anions, as this detecting system offers high efficiency, high sensitivity, easy operation and low cost.[11]

Manganese, the 12th most common element in the earth's crust, is abundantly present in the environment and our food, including nuts, grains, tea, and legumes, which provide an average daily intake of about 5 mg kg^{-1}.[12–14] Besides, manganese is an essential trace element and has important functions, such as in catalysis and as a structural component in diverse proteins, *e.g.* the photosynthetic apparatus and the enzyme superoxide dismutase.[15,16] However, an elevated level of manganese can result in toxic neurological effects, which cause a series of symptoms, such as adynamia/fatigability, sialorrhea, cephalalgia, sleep disturbances, muscular pain and hypertonia, masklike face, gait changes, reduced coordination, hallucinations, and mental irritability, finally leading to a Mn-induced Parkinson like disease, called manganism.[17] Furthermore,

manganese can exist in a wide range of oxidation states, *viz.* 2+, 3+, 4+, 5+, and 6+, and thus may promote redox reactions and form cytotoxic free radicals.[18–20] Among them, Mn^{2+} and Mn^{3+} have differential cytotoxicity. According to Zheng's report, Mn^{3+} species appeared to be more cytotoxic than Mn^{2+} ones in their *in vitro* study.[21] Therefore, the development of chemosensors for differentiating of Mn^{3+} from Mn^{2+} is highly significant and much needed. Nevertheless, the simultaneous detection of both Mn^{2+} and Mn^{3+} has not been reported yet, to the best of our knowledge.

In recent years, Dai and co-workers have reported a chromogenic sensor for determination of manganese ion, which was the first colorimetric chemosensor capable of detecting Mn^{2+} in aqueous solution.[22] Our group also developed two colorimetric chemosensors for detecting Mn^{2+}, which were successfully used to sense Mn^{2+} ions at a concentration below WHO guideline.[23,24]

To further develop a more selective and sensitive tool to identify and distinguish between Mn^{2+} and Mn^{3+} ions, herein we report a newly designed colorimetric chemosensor, which was based on Schiff base derivative containing diethylaminosalicyl moiety and have a strong chromogenic and binding properties. Specifically, chemosensor comprised of combination of 4-(diethylamino)salicylaldehyde and 2-(aminomethyl)benzenamine with high sensitivity and excellent selectivity in aqueous solution. The chemosensor **1** exhibited a color change from pale yellow to reddish brown upon binding to Mn^{2+} and Mn^{3+}, respectively, while **1** reacts with Mn^{3+} *ca.* 20 times faster than Mn^{2+}. The different reaction time of Mn(III) and Mn(II) with **1** was used to differentiate Mn(III) from Mn(II).

2. Experimental section

2.1 Materials and equipment

All the solvents and reagents (analytical and spectroscopic grade) were purchased from Sigma-Aldrich. ^{1}H and ^{13}C NMR

Department of Fine Chemistry and Department of Interdisciplinary Bio IT Materials, Seoul National University of Science and Technology, Seoul 139-743, Korea. E-mail: chealkim@seoultech.ac.kr; Fax: +82-2-973-9149; Tel: +82-2-970-6693
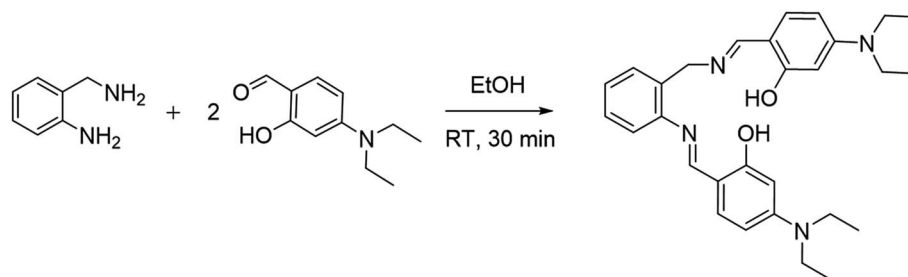
Scheme 1 Synthetic procedure of **1**.

spectra were recorded on a Varian 400 MHz and 100 MHz spectrometer and chemical shifts were recorded in ppm. Electro spray ionization mass spectra (ESI-MS) were collected on a Thermo Finnigan (San Jose, CA, USA) LCQ_{TM} Advantage MAX quadrupole ion trap instrument by infusing samples directly into the source using a manual method. Spray voltage was set at 4.2 kV, and the capillary temperature was at 80 °C. Absorption spectra were recorded at room temperature using a Perkin Elmer model Lambda 2S UV/Visible spectrometer. Elemental analysis for carbon, nitrogen, and hydrogen was carried out using a Flash EA 1112 elemental analyzer (thermo) at the Organic Chemistry Research Center of Sogang University, Korea. SW-EPR spectra were taken at 5 K using an X-band Bruker EMX-plus spectrometer equipped with a dual mode cavity (ER 4116DM). ICP-spectrometry analysis for Mn was performed using IRIS XDL Duo (Thermo Fisher Scientific).

2.2 Synthesis of sensor 1

An ethanolic solution of 4-(diethylamino)salicylaldehyde (0.39 g, 2 mmol) was added to 2-(aminomethyl)benzenamine (0.14 g, 1 mmol) in absolute ethanol (3 mL). The reaction solution was stirred for 30 min at room temperature and the solvent was removed *in vacuo*. The crude product was purified by column chromatography using hexane/ethyl acetate (2 : 1, v/v) as eluent. Yield 0.28 g (60%); ^{1}H NMR (400 MHz CD$_3$CN, ppm): δ 13.54 (s, 1H), 13.45 (s, 1H), 8.46 (s, 1H), 8.22 (s, 1H), 7.33 (m, 2H), 7.20 (m, 3H), 6.98 (d, $J = 8.8$ Hz, 1H), 6.30 (d, $J = 8.8$ Hz, 1H), 6.16 (d, $J = 8.8$ Hz, 1H), 6.12 (s, 1H), 5.96 (s, 1H), 4.75 (s, 2H), 3.39 (q, 4H), 3.32 (q, 4H), 1.13 (t, 6H), 1.05 (t, 6H); ^{13}C NMR (100 MHz DMSO-d_6, ppm):
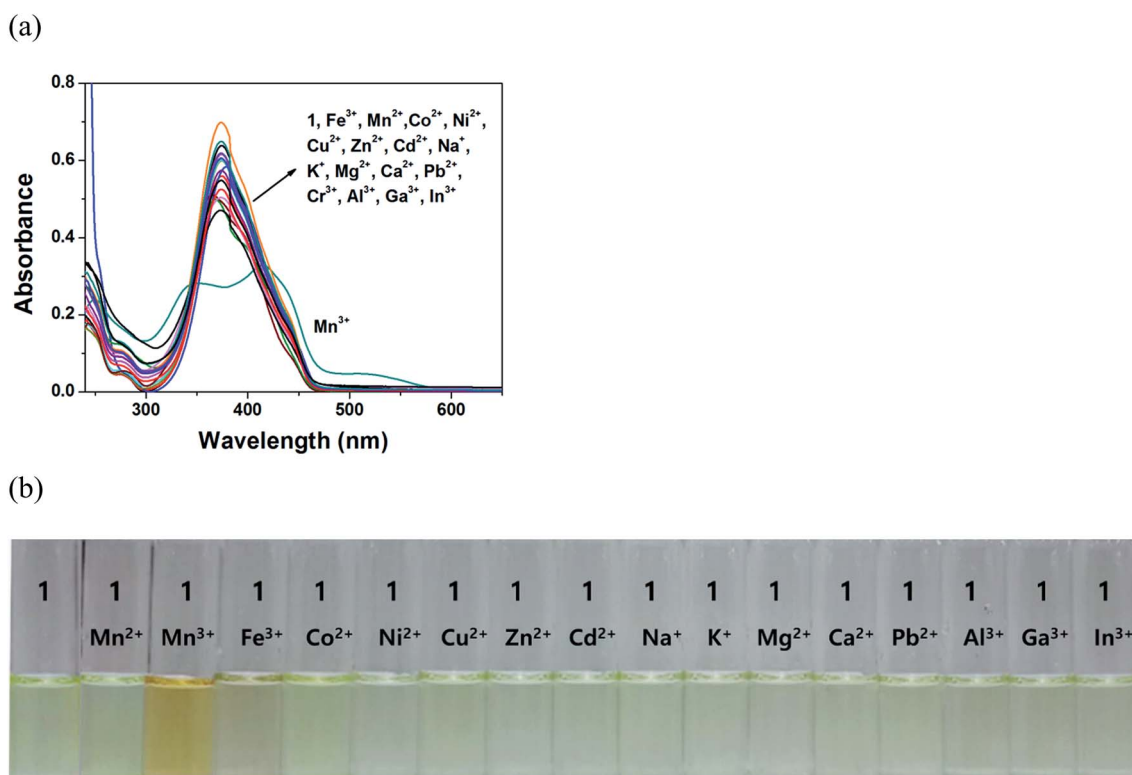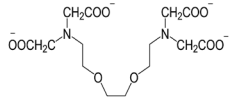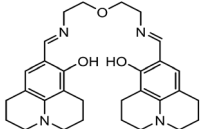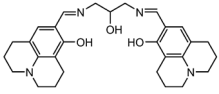
(a)

(b)
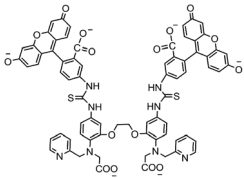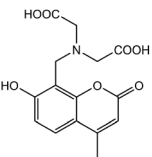
Fig. 1 (a) Absorption spectral changes of **1** (10 μM) upon the addition of 1.3 equiv. of various metal ions in 10 mM bis-tris buffer/CH$_3$CN (7 : 3, v/v). (b) The color changes of **1** (10 μM) upon the addition of 1.3 equiv. of various metal ions.

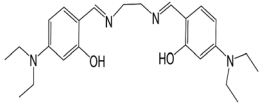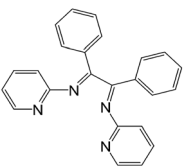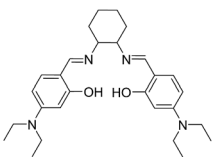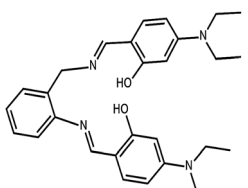164.68, 164.16, 163.07, 161.90, 151.58, 150.85, 147.18, 134.32, 133.02, 132.31, 128.82, 128.59, 125.63, 118.05, 108.79, 107.92, 103.84, 102.89, 97.18, 96.79, 57.51, 43.98, 43.80, 12.56. ESI-MS m/z (M + H$^+$): calcd, 473.29; found, 473.27. Anal. calc. for $C_{29}H_{36}N_4O_2$: C, 73.70; H, 7.68; N, 11.85%. Found: C, 73.43; H, 7.72; N, 12.07%.

2.3 UV-vis titrations

For Mn^{3+}: sensor **1** (1.4 mg, 0.003 mmol) was dissolved in CH$_3$CN (1 mL) and 10 μL of this solution (3 mM) was diluted with 2.99 mL of 10 mM bis-tris buffer/CH$_3$CN (7 : 3, v/v) to obtain a final concentration of 10 μM. Mn(OAc)$_3$·2H$_2$O (0.83

Table 1 Examples of some chemosensors for Mn^{2+} and Mn^{3+} detection

Sensor	Detection limit (μM)	Interference	Water% in solvent	Method of detection	Sensing metal ions	Reference
	No data	No data	100%	Naked eye	Mn^{2+} & Zn^{2+}	22
	6.03	Zn^{2+}, Cr^{3+}	10%	Naked eye	Mn^{2+}, Zn^{2+} & Al^{3+}	23
	7.11	Cu^{2+}, Co^{2+}	20%	Naked eye	Mn^{2+} & Fe^{2+}	24
	No data	Fe^{2+}, Co^{2+}, Zn^{2+}, Cd^{2+}, Hg^{2+}	100%	Fluorescence	Mn^{2+}, Fe^{2+}, Zn^{2+} & Cd^{2+}	34
	No data	Co^{2+}, Cu^{2+}, Fe^{2+}	100%	Fluorescence	Mn^{2+}	35
	1	Pb^{2+}	100%	Naked eye	Mn^{2+}	36
	No data	No data	50%	Fluorescence	Mn^{2+}	37
	5.0	Fe^{2+}, Co^{2+}	0%	Naked eye	Mn^{2+}	38
	0.91, 0.64	Co^{2+}, Cu^{2+}	70%	Naked eye	Mn^{2+} & Mn^{3+}	This work

mg, 0.003 mmol) was dissolved in CH_3CN (1 mL) and 1–13 μL of this Mn^{3+} solution (1 mM) was transferred to each sensor solution (10 μM) to give 1–1.3 equiv. After mixing them for 10 min, UV-vis spectra were taken at room temperature.

For Mn^{2+}: sensor **1** (1.4 mg, 0.003 mmol) was dissolved in CH_3CN (1 mL) and 10 μL of this solution (3 mM) was diluted with 2.99 mL of 10 mM bis-tris buffer/CH_3CN (7 : 3, v/v) to make the final concentration of 10 μM. $Mn(OAc)_2 \cdot 4H_2O$ (0.74 mg, 0.003 mmol) was dissolved in CH_3CN (1 mL) and 1–13 μL of this Mn^{2+} solution (1 mM) was transferred to each sensor solution (10 μM) to give 1–1.3 equiv. After mixing them for 4 h, UV-vis spectra were taken at room temperature.

2.4 Job plot measurements

For Mn^{3+}: sensor **1** (1.4 mg, 0.003 mmol) was dissolved in CH_3CN (1 mL). The following aliquots of the above **1** solution were transferred to separate vials: 12, 10.8, 9.6, 8.4, 7.2, 6.0, 4.8, 3.6, 2.4, 1.2 and 0 μL. $Mn(OAc)_3 \cdot 2H_2O$ (0.83 mg, 0.003 mmol) was dissolved in bis-tris buffer/CH_3CN (7 : 3, v/v, 1 mL). Volumes of the Mn^{3+} solution were added to each of the above vials containing **1** solution: 0, 1.2, 2.4, 3.6, 4.8, 6.0, 7.2, 8.4, 9.6, 10.8 and 12 μL. Each vial was then diluted with bis-tris buffer/CH_3CN (7 : 3, v/v) to obtain a total volume of 3 mL. After reacting them for 10 min, UV-vis spectra were taken at room temperature.

For Mn^{2+}: sensor **1** (1.4 mg, 0.003 mmol) was dissolved in CH_3CN (1 mL). The following aliquots of the above **1** solution were transferred to separate vials: 12, 10.8, 9.6, 8.4, 7.2, 6.0, 4.8, 3.6, 2.4, 1.2 and 0 μL. $Mn(OAc)_2 \cdot 4H_2O$ (0.74 mg, 0.003 mmol) was dissolved in bis-tris buffer/CH_3CN (7 : 3, v/v, 1 mL). Volumes of the Mn^{2+} solution were added to each of the above vials containing **1** solution: 0, 1.2, 2.4, 3.6, 4.8, 6.0, 7.2, 8.4, 9.6, 10.8 and 12 μL. Each vial was further diluted with bis-tris buffer/CH_3CN (7 : 3, v/v) to obtain a total volume of 3 mL. After reacting them for 4 h, UV-vis spectra were taken at room temperature.

2.5 Competition with other metal ions

Sensor **1** (1.4 mg, 0.003 mmol) was dissolved in CH_3CN (1 mL) and 10 μL of this solution (3 mM) was diluted with 2.99 mL of 10 mM bis-tris buffer/CH_3CN (7 : 3, v/v) to make the final concentration of 10 μM. MNO_3 (M = Na, K, 0.003 mmol) or $M(NO_3)_2$ (M = Co, Ni, Cu, Zn, Cd, Mg, Ca, Pb, 0.003 mmol) or $M(NO_3)_3$ (M = Fe, Cr, Al, Ga, In, 0.003 mmol) was dissolved in CH_3CN (1 mL), separately. Each metal solution (13 μL, 3 mM) was then added to 3 mL of the solution of sensor **1** (10 μM) to give 1.3 equiv. of the metal ions. Then, 13 μL of Mn^{3+} solution (3 mM) was added into the mixed solution of each metal ion and **1** to make 1.3 equiv. After mixing them for 10 min, UV-vis spectra were recorded at room temperature.

2.6 Study on the effect of pH

A series of buffers with pH values ranging from 2 to 12 was prepared by mixing sodium hydroxide solution and hydrochloric acid in bis-tris buffer. After the solution reached the desired pH, **1** (1.4 mg, 0.003 mmol) was dissolved in CH_3CN (1 mL), and then 10 μL of the sensor **1** solution (3 mM) was diluted with 2.99 mL buffers to make the final concentration of 10 μM. $Mn(OAc)_3 \cdot 2H_2O$

(0.83 mg, 0.003 mmol) was dissolved in bis-tris buffer (1 mL, pH 7). Next, 13 μL of the Mn^{3+} solution (3 mM) was transferred to each receptor solution (10 μM) prepared above. After mixing them for 10 min, UV-vis spectra were run at room temperature.

2.7 EDTA reversibility

The sensor **1** (1.4 mg, 0.003 mmol) was dissolved in CH_3CN (1 mL) and 10 μL (3 mM) of the **1** solution was diluted with 2.99 mL bis-tris buffer/CH_3CN (7 : 3, v/v) to make a final concentration of 10 μM. $Mn(OAc)_3 \cdot 2H_2O$ (0.83 mg, 0.003 mmol) was dissolved in bis-tris buffer (1 mL) and 13 μL of the Mn^{3+} solution (3 mM) was added to the solution of **1** (10 μM) prepared above. After mixing it for 10 min, UV-vis spectrum was recorded at room temperature. Ethylenediaminetetraacetic acid disodium salt dehydrate (EDTA, 0.88 mg, 0.003 mmol) was dissolved in bis-tris (1 mL) and 13 μL of the EDTA solution (3 mM) was added to the solution of **1**–Mn^{3+} complex (10 μM) prepared above. After mixing it for 1 min, UV-vis spectrum was again recorded. For the reversibility study, another 13 μL of the Mn^{3+} solution (3 mM) was added to the above solution. After mixing it for 10 min, UV-vis spectrum was run at room temperature. The same experimental procedure was repeated one more time.

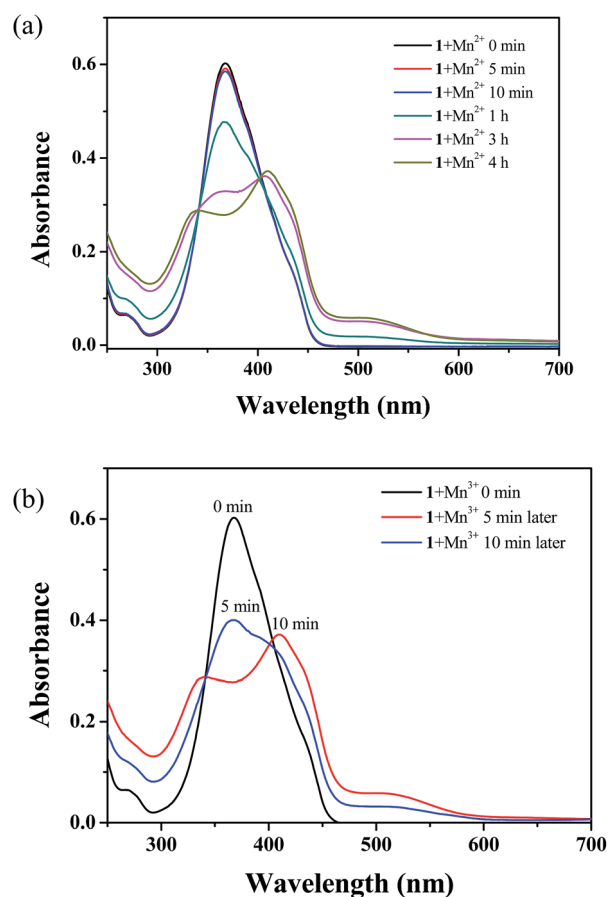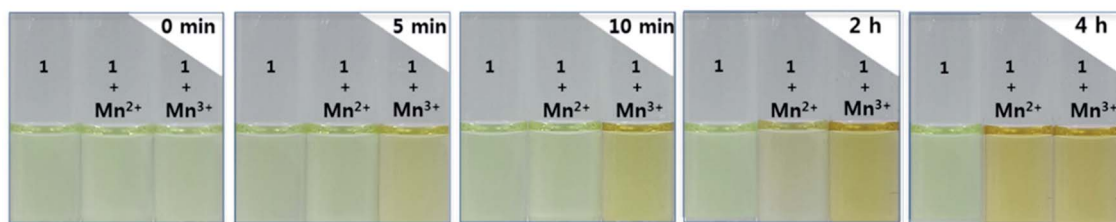Fig. 2 (a) Time-dependent absorption spectral changes of **1** (10 μM) upon addition of 1.3 equiv. of $Mn(OAc)_2$ from 0 to 4 h. (b) Time-dependent absorption spectral changes of **1** (10 μM) upon addition of 1.3 equiv. of $Mn(OAc)_3$ from 0 to 10 min.

(a)

(b)

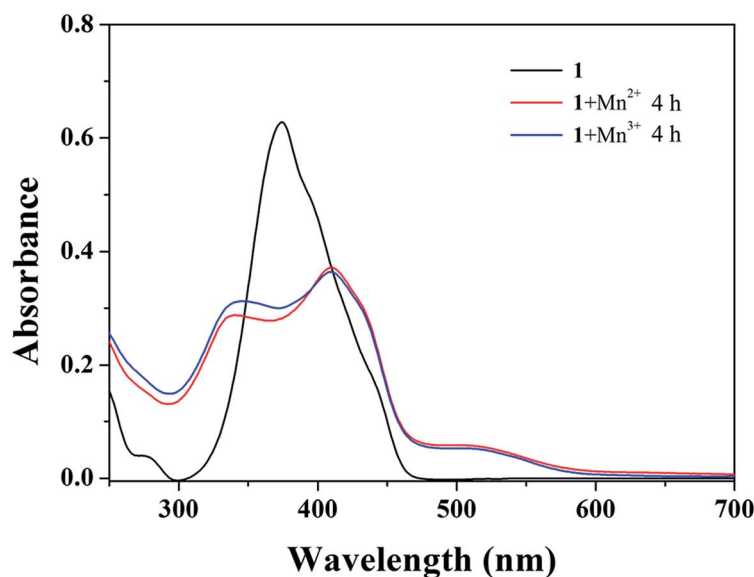Fig. 3 (a) Time-dependent color changes of **1** (10 μM) upon addition of 1.3 equiv. of $Mn(OAc)_2$ and $Mn(OAc)_3$, respectively. (b) UV-vis spectra of **1** (10 μM) 4 h after 1.3 equiv. of Mn^{2+} and Mn^{3+} were added into **1**, respectively.

2.8 Colorimetric test strips towards metal ions

Sensor **1** (14.2 mg, 0.03 mmol) was dissolved in CH_3CN (1 mL). The sensor **1**-test kits were prepared by immersing filter papers into **1** solution (30 mM), and then dried in air. MNO_3 (M = Na, K: 0.05 μmol), $M(NO_3)_2$ (M = Co, Ni, Cu, Zn, Cd, Mg, Ca, Pb: 0.05 μmol), $M(NO_3)_3$ (M = Al, Fe, Cr, Ga, In: 0.05 μmol) or $M(OAc)_3$ (M = Mn) was separately dissolved in buffer (1 mL). The test strips prepared above were added into different metal solutions (50 μM), and then dried at room temperature.

2.9 Determination of Mn^{3+} in water samples

UV-vis spectral measurement of water samples containing Mn^{3+} was carried by adding 30 μL of 3 mmol L^{-1} stock solution of **1** and 0.60 mL of 50 mmol L^{-1} bis-tris buffer/CH_3CN (7 : 3, v/v) stock solution to 2.37 mL sample solutions. After well mixed, the solutions were allowed to stand at 25 °C for 10 min before the test. Sewage water samples were centrifuged for 20 min (2100 RCF) and only the supernatant was used for ICP spectrometry analysis.
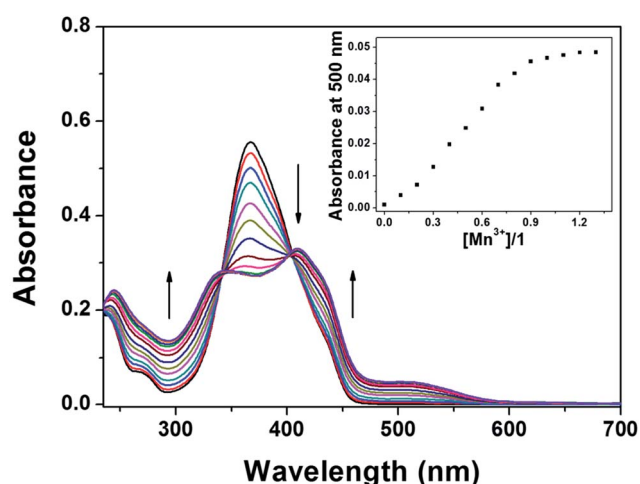

Fig. 4 Absorption spectral changes of **1** (10 μM) after addition of increasing amounts of Mn^{3+} (0.1, 0.2, 0.3, 0.4, 0.5, 0.6, 0.7, 0.8, 0.9, 1, 1.1, 1.2 and 1.3 equiv.) in 10 mM bis-tris buffer/CH_3CN (7 : 3, v/v) at room temperature. Inset: absorption at 500 nm *versus* the number of equiv. of Mn^{3+} added.
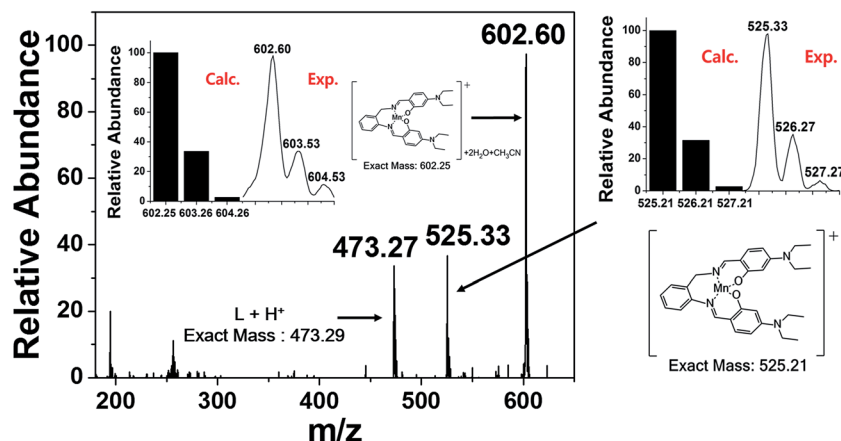
Fig. 5 Positive-ion electrospray ionization mass spectrum of **1** (100 μM) upon addition of 1 equiv. of Mn^{3+}.

2.10 Theoretical calculation methods

All DFT/TDDFT calculations based on the hybrid exchange-correlation functional B3LYP[25,26] were carried out using Gaussian 03 program.[27] The 6-311+G** basis set was used for the main group elements, whereas the Lanl2DZ effective core potential (ECP)[28–30] was employed for Mn. In vibrational frequency calculations, there was no imaginary frequency for the optimized geometries of **1** and 1^{2-}–Mn^{3+}, suggesting that those geometries represented local minima. For all calculations, the solvent effect of water was considered by using the Cossi and Barone's CPCM (conductor-like polarizable continuum model).[31,32] To investigate the electronic properties of singlet excited states, time-dependent DFT (TDDFT) was performed in the ground state geometries of **1** and 1^{2-}–Mn^{3+}. Forty lowest singlet states were calculated and analyzed. The GaussSum 2.1 (ref. 33) was used to calculate the contributions of molecular orbital in electronic transitions.

3. Results and discussion

3.1 Synthesis of sensor 1

Sensor **1** was obtained by the combination of 4-(diethylamino) salicylaldehyde and 2-(aminomethyl)benzenamine with 60% yield in ethanol (Scheme 1), and characterized by ^{1}H NMR and ^{13}C NMR, ESI-mass spectrometry, and elemental analysis.

3.2 Spectral and colorimetric response of 1 toward Mn^{3+}

The selectivity of sensor **1** toward various metal cations, Na^+, K^+, Mg^{2+}, Ca^{2+}, Cr^{3+}, Mn^{2+}, Mn^{3+}, Fe^{3+}, Co^{2+}, Ni^{2+}, Cu^{2+}, Zn^{2+}, Cd^{2+}, Al^{3+}, Ga^{3+}, In^{3+} and Pb^{2+} was primarily studied by UV-vis spectroscopy in bis-tris buffer/CH_3CN (7 : 3, v/v). Upon the addition of 1.3 equiv. of each cation, **1** showed little or no spectra changes in absorption peaks in the presence of Na^+, K^+, Mg^{2+}, Ca^{2+}, Cr^{3+}, Mn^{2+}, Fe^{3+}, Co^{2+}, Ni^{2+}, Cu^{2+}, Zn^{2+}, Cd^{2+}, Al^{3+}, Ga^{3+}, In^{3+} and Pb^{2+} (Fig. 1a). By contrast, the addition of Mn^{3+} to **1** caused a significant spectral change and showed a color change from pale yellow to reddish brown within 10 min (Fig. 1b). Importantly, this is the first example for the detection of Mn^{3+} in aqueous solution (Table 1), to the best of our knowledge.

More importantly, **1** could also detect Mn^{2+} with longer sensing time (4 h) as shown in Fig. 2. The reaction of Mn^{2+} with **1** was very slow and took 4 h for the complete reaction (Fig. 2a), while its reaction with Mn^{3+} finished within 10 min (Fig. 2b). Consistent with UV-vis study, the solution color of **1** in the presence of Mn^{2+} slowly changed to reddish brown (Fig. 3a). The solution color of **1**–Mn^{2+} complex 4 h after **1** was mixed with Mn^{2+} was eventually the same as that of **1** with Mn^{3+}, indicating that the **1**–Mn^{2+} complex might be oxidized to the **1**–Mn^{3+} complex with the same color change from pale yellow to reddish brown. Also, UV-vis absorption spectra of **1**–Mn^{2+} and **1**–Mn^{3+} complexes 4 h after **1** reacted with Mn^{2+} and Mn^{3+}, respectively, supported this proposal (Fig. 3b). At this stage, we do not understand why Mn^{2+} and Mn^{3+} are more selective towards the
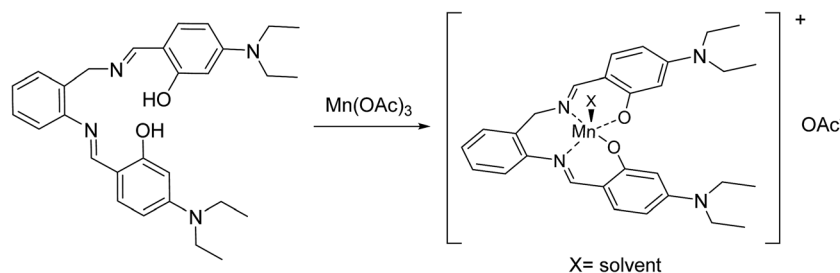
Scheme 2 Proposed structure of **1**–Mn^{3+} complex.

sensor **1** in comparison with other ions. Importantly, the colorimetric discrimination of Mn^{3+} from Mn^{2+} is also the first example, to the best of our knowledge (Table 1).

First of all, the binding properties of **1** with Mn^{3+} were studied by UV-vis titration experiments (Fig. 4). On sequential addition of Mn^{3+} to a solution of **1**, the absorption band at 361 nm decreased and two new bands at 300 nm and 500 nm

gradually reached maxima at 1.3 equiv. These peaks with molar extinction coefficients in the thousands, 1.4×10^5 M^{-1} cm^{-1} $(\varepsilon_{300 \text{ nm}})$ and 7.0×10^4 M^{-1} cm^{-1} $(\varepsilon_{463 \text{ nm}})$, were too large to be Mn-based d–d transitions. Thus, the peak at 500 nm might be attributed to a ligand-to-metal charge-transfer (LMCT),[38–41] which is responsible for the reddish brown color of the solution. Meanwhile, an isosbestic point was observed at 341 nm,

(a)

(b)

(c)

Fig. 6 (a) Absorption spectral changes of competitive selectivity of **1** (10 µM) toward Mn^{3+} (1.3 equiv.) in the presence of other metal ions (1.3 equiv.). (b) Bar graphs of competitive selectivity of **1** (10 µM) toward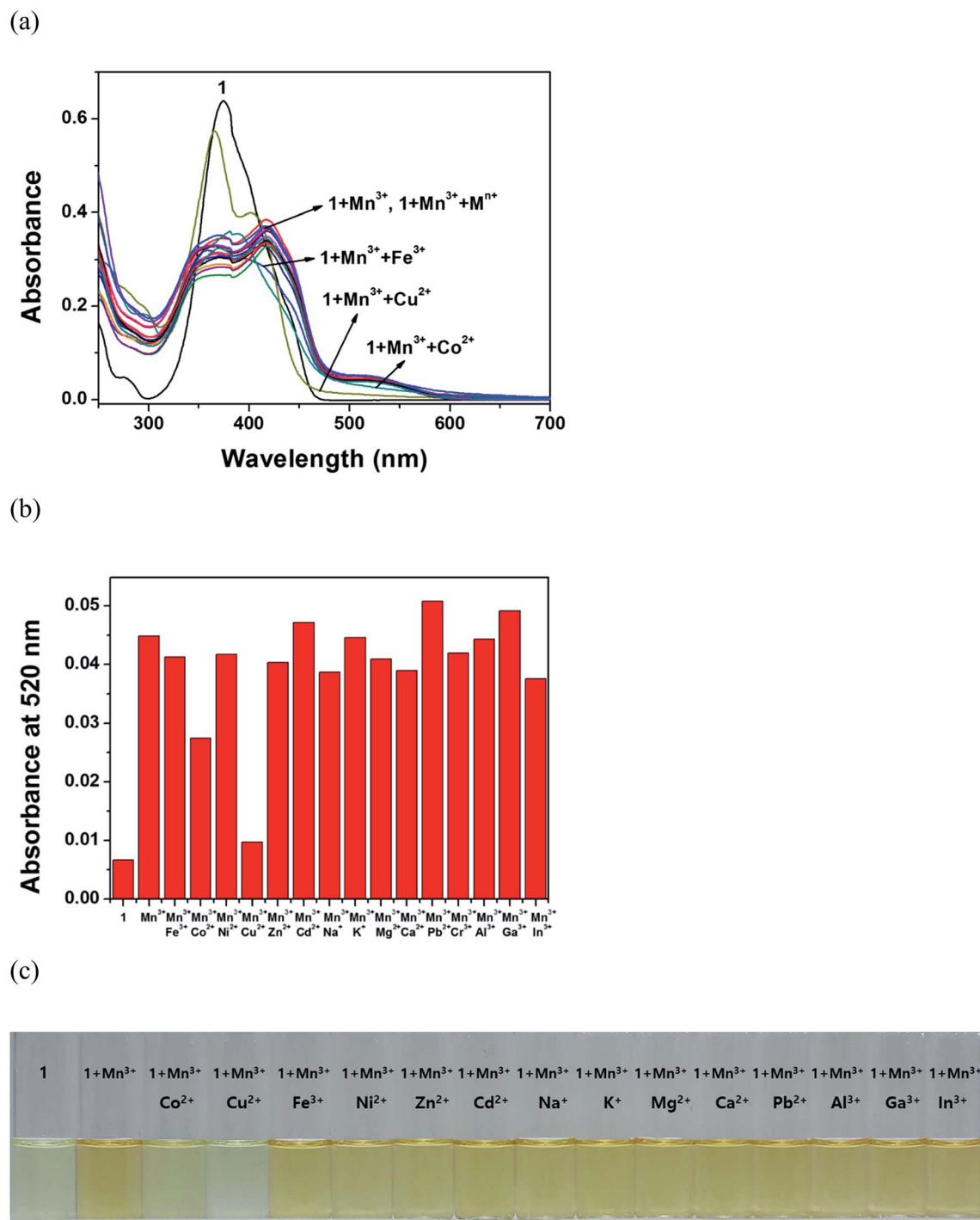s Mn^{3+} (1.3 equiv.) in the presence of other metal ions (1.3 equiv.). (c) The color changes of competitive selectivity of **1** (10 µM) toward Mn^{3+} (1.3 equiv.) in the presence of other metal ions (1.3 equiv.).

demonstrating that only one product was generated from **1** upon binding to Mn^{3+}. These results indicated that sensor **1** could serve as a selective chromogenic sensor for Mn^{3+} ion.

The binding mode between **1** and Mn^{3+} was determined through Job plot analysis (Fig. S1†),[42] which exhibited a 1 : 1 complexation stoichiometry for the **1**–Mn^{3+} complex formation. To further confirm the binding mode between **1** and Mn^{3+}, ESI-mass spectrometry analysis was carried out (Fig. 5). The positive-ion mass spectrum indicated that the peak at $m/z =$ 525.33 was assignable to $[\mathbf{1}-2H^+ + Mn^{3+}]^+$ [calcd, 525.21] and the peak at $m/z = $ 602.60 assignable to $[\mathbf{1}-2H^+ + Mn^{3+} + 2H_2O + CH_3CN]^+$ [calcd, 602.25] complex. Based on Job plot and ESI-mass spectrometry analysis, we propose the structure of **1**–Mn^{3+} complex as shown in Scheme 2.

The binding constant of **1** with Mn^{3+} was calculated as 5.0×10^4 M^{-1} on the basis of Benesi–Hildebrand equation (Fig. S2†).[43] Based on the result of UV-vis titration, the detection limit for Mn^{3+} was determined to be 0.64 μM on the basis of definition by IUPAC ($C_{DL} = 3S_b/m$, Fig. S3†). Importantly, the value (0.64 μM) for Mn^{3+} is much below the World Health Organization (WHO) guideline (7.28 μM) in the drinking water and the lowest among those previously reported for Mn$^{2+/3+}$-binding chemosensors in aqueous solution, to the best of our knowledge.[44] This result indicated that **1** could be a powerful tool for the detection of Mn^{3+} in the drinking water.

To check further the practical applicability of receptor **1** as a Mn^{3+}-selective receptor, we carried out competition experiment (Fig. 6). A background of most coexistent metal ions such

(a)

(b)

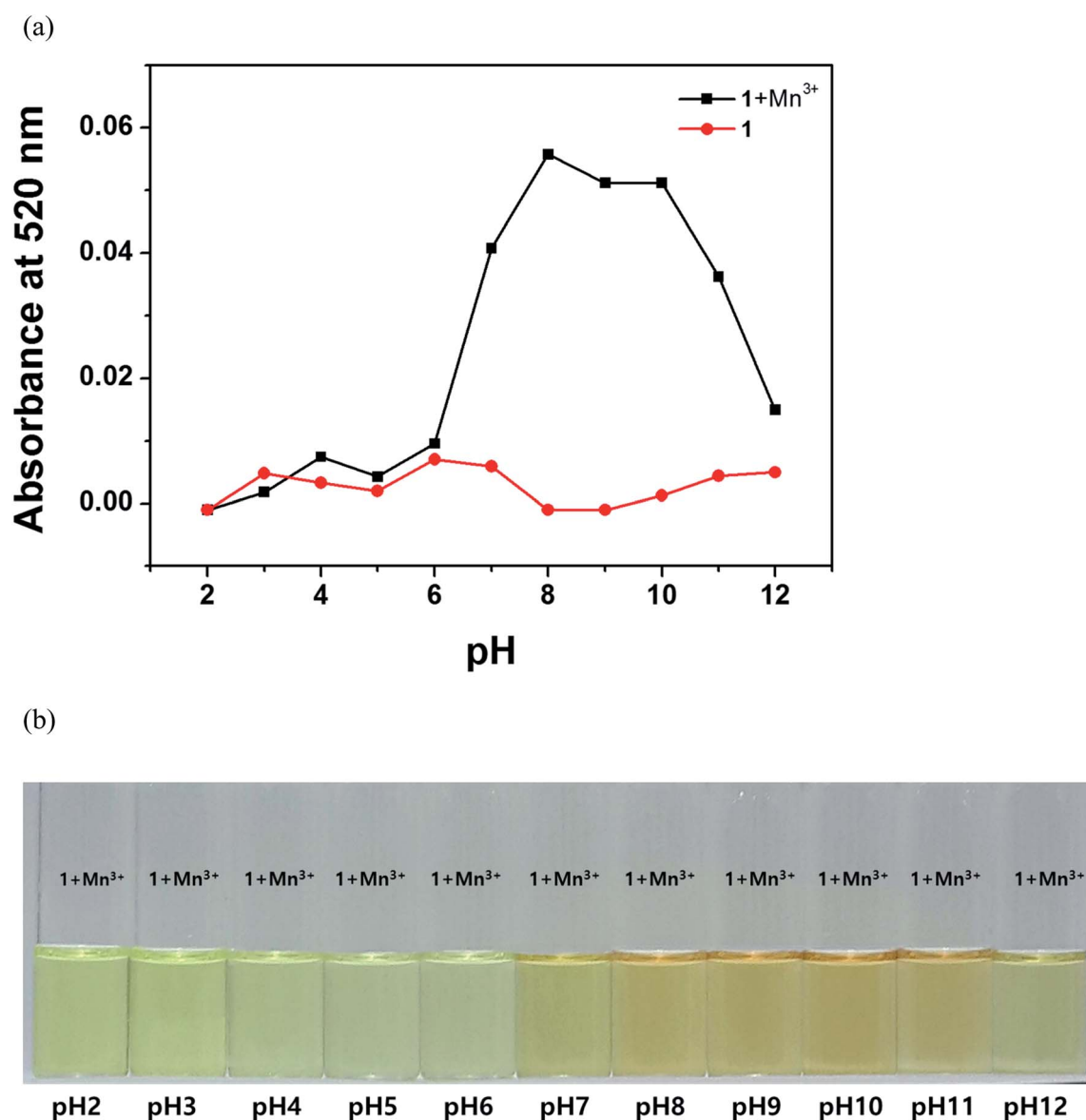**Fig. 7** (a) Absorbance intensities (at 520 nm) of **1**–Mn^{3+} complex (**1** = 10 μM) after addition of 1.3 equiv. of Mn^{3+} at various range of pH in bis-tris buffer/CH$_3$CN (7 : 3, v/v) at room temperature. (b) The color changes of **1**–Mn^{3+} complex (**1** = 10 μM) after addition of 1.3 equiv. of Mn^{3+} at various range of pH in bis-tris buffer/CH$_3$CN (7 : 3, v/v) at room temperature.

as Na^+, K^+, Mg^{2+}, Ca^{2+}, Cr^{3+}, Fe^{3+}, Co^{2+}, Ni^{2+}, Cu^{2+}, Zn^{2+}, Cd^{2+}, Al^{3+}, Ga^{3+}, In^{3+} and Pb^{2+} did not interfere with the detection of Mn^{3+} by 1 in bis-tris buffer/CH_3CN (7 : 3, v/v). However, Co^{2+} and Cu^{2+} quenched about 46% and 92% of the absorbance obtained with Mn^{3+} alone, respectively, suggesting that Co^{2+} and Cu^{2+} have a comparable or stronger binding ability to 1 compared to Mn^{3+}. These results indicated that 1 could be an excellent chromogenic sensor for Mn^{3+} over most competing relevant metal ions, in spite of interfering with Co^{2+} and Cu^{2+}, in aqueous solution. To overcome the interference of Co^{2+} and Cu^{2+}, cyanide was used as binding agent for Co^{2+} and Cu^{2+} (Fig. S4†). The detection of Mn^{3+} with 1 was not interfered by both Co^{2+} and Cu^{2+} in presence of the CN^- ion.

For environmental applications, the pH dependence of the 1–Mn^{3+} complex was further investigated, as shown in Fig. 7. Over the pH range tested, the absorbance intensity of the complex displayed a strong pH dependence. As the nitrogen atoms of imine groups of 1 could be protonated below pH 6.0, 1 might not chelate with Mn^{3+}. At pH higher than 11.0, 1–Mn^{3+} complex may decompose by demetallation. Therefore, an intense and stable absorption intensity of 1–Mn^{3+} complex was observed in the pH range of 7.0–11.0, which warrants its application in monitoring Mn^{3+} by naked-eye without having it affected by changes in physiological pH values.

To examine the reversibility of sensor 1 toward Mn^{3+} in bis-tris buffer/CH_3CN (7 : 3, v/v), ethylenediaminetetraacetic acid (EDTA, 1.3 equiv.) was added to the solution of sensor 1 and Mn^{3+} complex. As shown in Fig. 8, the addition of EDTA to a mixture of 1 and Mn^{3+} resulted in a return of the absorbance from reddish brown to pale yellow at 450 nm, which indicated the regeneration of the free 1. Upon re-addition of Mn^{3+} into the solution, the color and the absorbance again changed to reddish brown. The absorbance and color changes were almost reversible even after several cycles with the sequential alternate addition of Mn^{3+} and EDTA. These results indicated that sensor 1 could be recyclable simply through treatment with a proper reagent such as EDTA. Such reversibility and regeneration could be important for the fabrication of chemosensors to sense Mn^{3+}.

For the practical application of sensor 1, test strips were prepared by immersing filter papers in the solution of 1 and then dried in air. These test strips were used to sense Mn^{3+} among different cations. As shown in Fig. 9, when the test strips coated with 1 were added to different cation solutions, a clear color change was observed only with Mn^{3+} in bis-tris buffer. Therefore, the test strips coated with the receptor 1 solution would be convenient for detecting Mn^{3+}. These results showed that receptor 1 could have a practical application for detecting Mn^{3+} in environmental samples. Moreover, this is the first example that the test strips were used to sense Mn^{3+} among different cations, to the best of our knowledge.

In order to examine the applicability of the chemosensor 1 in environmental samples, we constructed a calibration curve for the determination of Mn^{3+} by 1 (Fig. S5†), which exhibited a good linear relationship between the absorbance of 1 and Mn^{3+} concentration (0.00–10.00 μM) with a correlation coefficient of $R^2 = 0.9971$ ($n = 3$). Then, the chemosensor was

applied to the determination of Mn^{3+} in water samples. First, tap water samples were chosen. As shown in Table 2, one can see that satisfactory recovery and R.S.D. values of water samples were exhibited. Second, artificial polluted water samples were prepared by adding various metal ions that are
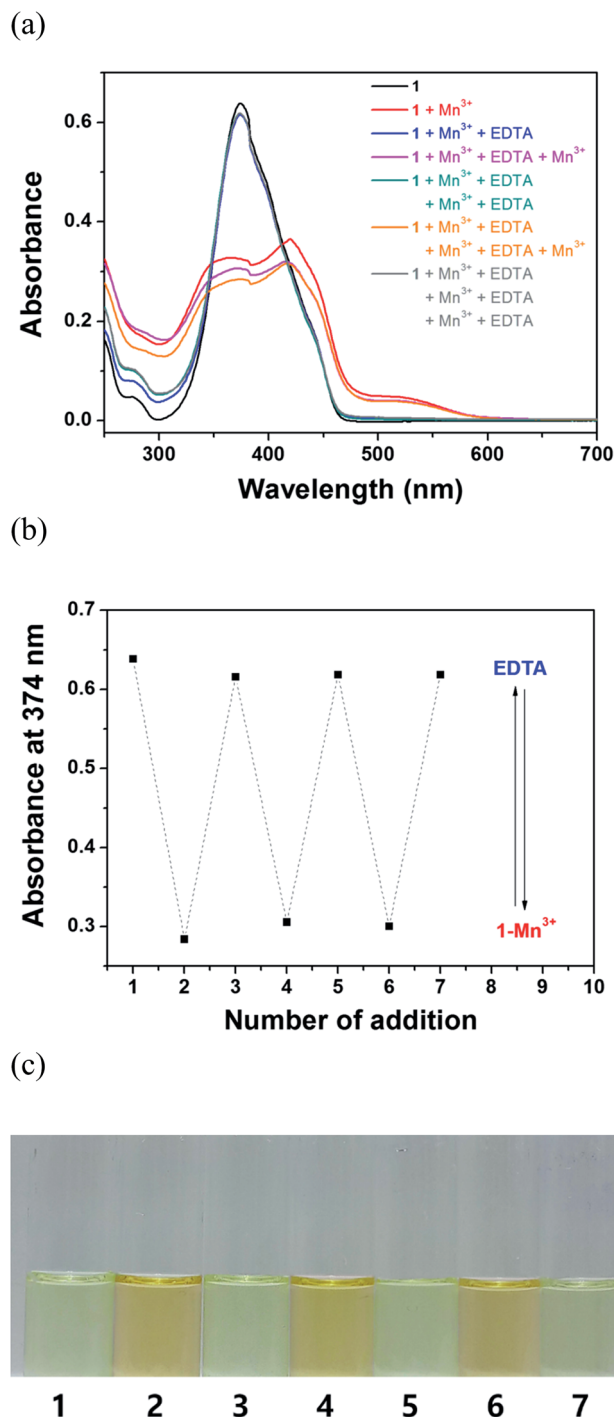

Fig. 8 (a) UV-vis spectral changes of 1 (10 μM) after the sequential addition of Mn^{3+} and EDTA. (b) Reversible changes in absorbance of 1 (10 μM) at 374 nm after the sequential addition of Mn^{3+} and EDTA. (c) The color changes of 1 (10 μM) after the sequential addition of Mn^{3+} and EDTA.
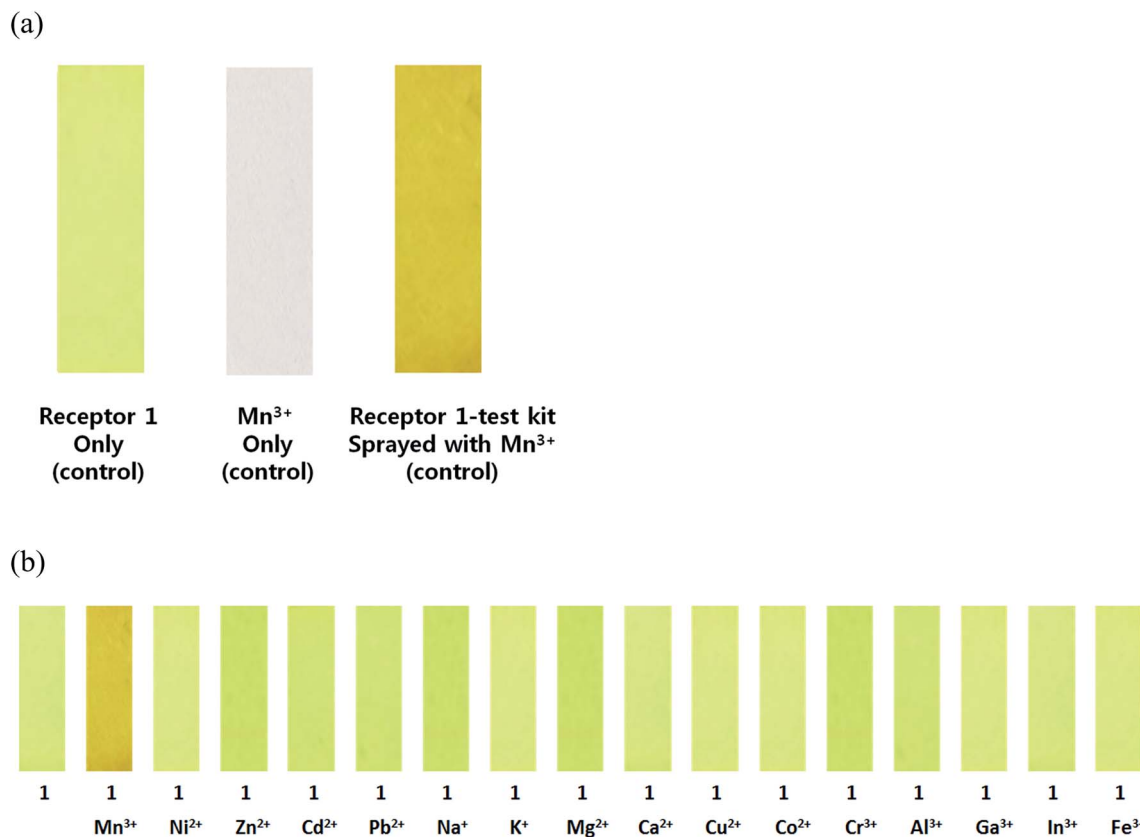
Fig. 9 Photographs of the filter paper coated with **1** used for the detection of Mn^{3+}. (a) Left to right: test kit coated with only receptor **1** (control, 10 mM), test kit coated with only Mn^{3+} (control, 50 μM), and receptor-**1** test kit immersed in Mn^{3+} solution. (b) Receptor-**1** test kits (10 mM) immersed in various metal ions (50 μM).

known to be involved in industrial processes into deionized water. The results have also been summarized in Table 2, which exhibited satisfactory recovery and R.S.D. values for all the water samples. In order to prove the validation of **1** as an analytical method for quantification, sewage water samples were chosen. **1** presented the comparable results with those of ICP-spectrometry analysis (Table 2), indicating that **1** could be used as an analytical method for detecting Mn^{3+} in real water samples.

3.3 Spectral and colorimetric response of 1 toward Mn^{2+}

To investigate the binding properties of **1** with Mn^{2+}, we carried out UV-vis titration experiments (Fig. 10). With gradual addition of Mn^{2+} to a solution of **1**, the absorption band at 372 nm significantly decreased and two new bands at 300 nm and 500 nm gradually reached maxima at 1.3 equiv. of Mn^{2+} with 4 h reaction time. A clear isosbestic point was observed at 350 nm, demonstrating that only one product was generated from **1** upon binding to Mn^{2+}. These observations were nearly identical to those of **1** with Mn^{3+}, except for a longer reaction time (10 m

Table 2 Determination of Mn(III) in water samples

Sample	Mn(III) added (μmol L^{-1})	Mn(III) found (μmol L^{-1})	Recovery^f (%)	R.S.D.^{g} (n = 3) (%)
Tap water^a	0.00	0.00	—	—
	6.00	5.78	96.6	3.0
Water sample^b	0.00	5.10	102	2.1
	2.00	7.41	115	2.2
Sewage water sample^c	0.00	3.63^d	—	3.5
	0.00	3.51^e	—	2.6

^{a} Tap water (10 mM bis-tris solution) : CH$_3$CN = 7 : 3, v/v. ^{b} Prepared by deionized water, 5.00 μmol L^{-1} Mn(III), 5 μmol L^{-1} Cd(II), Pb(II), Na(I), K(I), Ca(II), Mg(II), Zn(II). Conditions: [**1**] = 30 μmol L^{-1} in 10 mM bis-tris buffer–CH$_3$CN solution (7 : 3, pH 7.0). ^{c} Sewage water was obtained from the pigsty in Seoul, Korea. ^{d} Our method. ^{e} Inductively Coupled Plasma (ICP) spectrometry analysis. ^{f} [(Mn(III) found)/(Mn(III) added)] × 100. ^{g} Relative standard deviations.
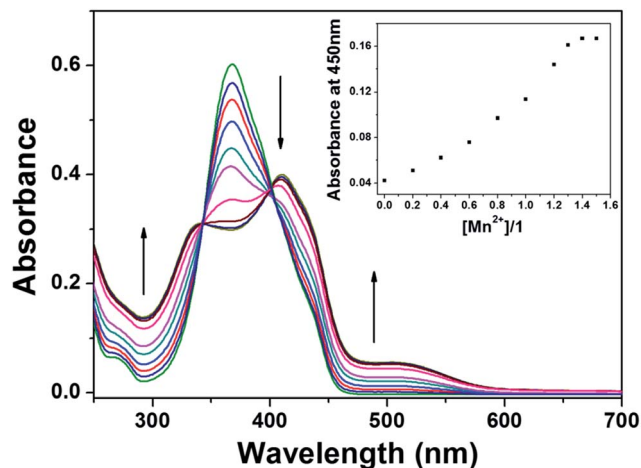
Fig. 10 Absorption spectral changes of **1** (10 μM) after addition of increasing amounts of Mn²⁺ (0.1, 0.2, 0.3, 0.4, 0.5, 0.6, 0.7, 0.8, 0.9, 1, 1.1, 1.2 and 1.3 equiv.) in 10 mM bis-tris buffer/CH₃CN (7 : 3, v/v) at room temperature. Inset: absorption at 463 nm *versus* the number of equiv. of Mn²⁺ added.

for Mn³⁺ *vs.* 4 h for Mn²⁺). These results indicated that receptor **1** could also serve as a selective chromogenic sensor for Mn²⁺ and discriminate Mn²⁺ from Mn³⁺ by the difference of the reaction time.

The binding mode between **1** and Mn²⁺ was determined through Job plot analysis (Fig. S6†).[42] The Job plot exhibited a 1 : 1 complexation stoichiometry for the **1**–Mn²⁺ complex formation. To further confirm the binding mode between **1** and Mn²⁺, ESI-mass spectrometry analysis was carried out (Fig. S7†). The positive-ion mass spectrum of **1**–Mn²⁺ complex was nearly identical to that of **1**–Mn³⁺ complex, although Mn²⁺ was used as standard metal ion. These results led us to propose two possibilities: one is that **1**–Mn²⁺ complex might be oxidized to the **1**–Mn³⁺ complex under ESI-mass experimental conditions, and the other is that after its formation from the reaction of Mn²⁺ with **1**, the **1**–Mn²⁺ complex is oxidized to the **1**–Mn³⁺ complex.

To investigate the correct reason, we first carried out the sensing test of **1**–Mn²⁺ and **1**–Mn³⁺ complexes under degassed conditions. If there is no color change for the complexation of the Mn²⁺ ion with **1** under the degassed conditions, it would mean that **1** detects Mn³⁺, not Mn²⁺, because **1**–Mn²⁺ complex is oxidized to **1**–Mn³⁺ complex only by O₂ molecules without any oxidants. Finally, we observed no color change for **1**–Mn²⁺ complex under the degassed conditions as shown in Fig. 11, while the solution of **1**–Mn³⁺ complex showed the color change from pale yellow to reddish brown. These results strongly

(a)

(b)
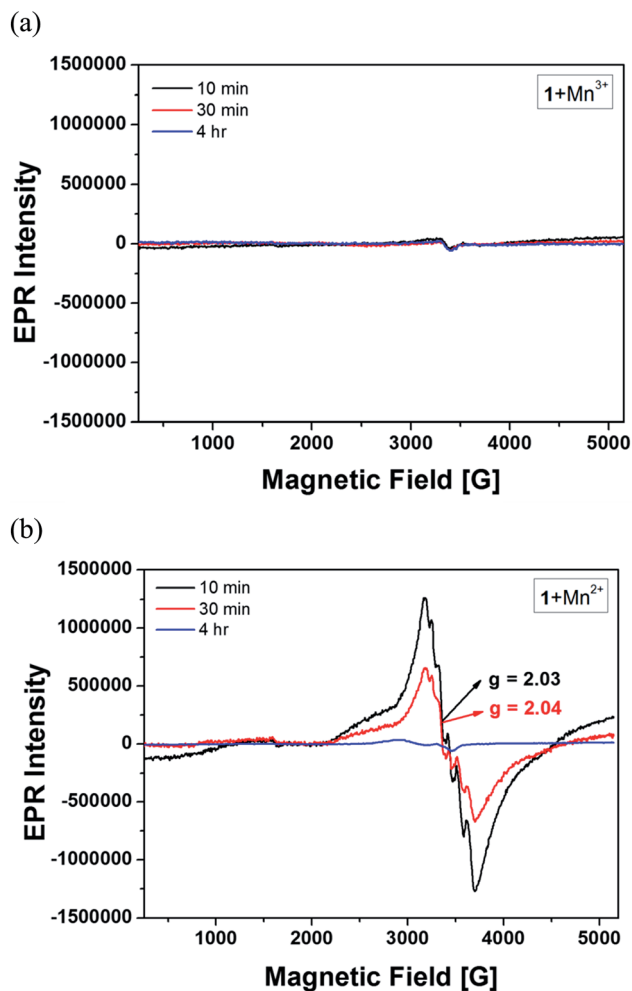
Fig. 12 X-band EPR spectra of **1**–Mn³⁺ and **1**–Mn²⁺ complexes recorded at 5 K: (a) the EPR samples were frozen in liquid nitrogen 10 m, 30 m and 4 h after **1** was mixed with Mn(OAc)₃ in CH₃CN/10 mM bis-tris buffer (3 : 7) at room temperature. The experimental parameters: microwave frequency = 9.647 (10 m), 9.647 (30 m), 9.648 (4 h) GHz, microwave power = 1.017 (10 m), 0.998 (30 m), 1.001 (4 h) mW, modulation amplitude = 10 G (10 m, 30 m, 4 h), gain = 1 × 10⁴ (10 m, 30 m, 4 h). (b) The EPR samples were frozen in liquid nitrogen 10 m, 30 m and 4 h after **1** was mixed with Mn(OAc)₂ in CH₃CN/10 mM bis-tris buffer (3 : 7) at room temperature. The experimental parameters: microwave frequency = 9.646 (10 m), 9.649 (30 m), 9.647 (4 h) GHz, microwave power = 0.991 (10 m), 0.999 (30 m), 0.996 (4 h) mW, modulation amplitude = 10 G (10 m, 30 m, 4 h), gain = 1 × 10⁴ (10 m, 30 m, 4 h).

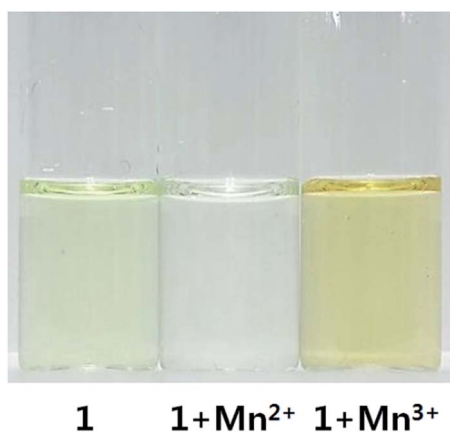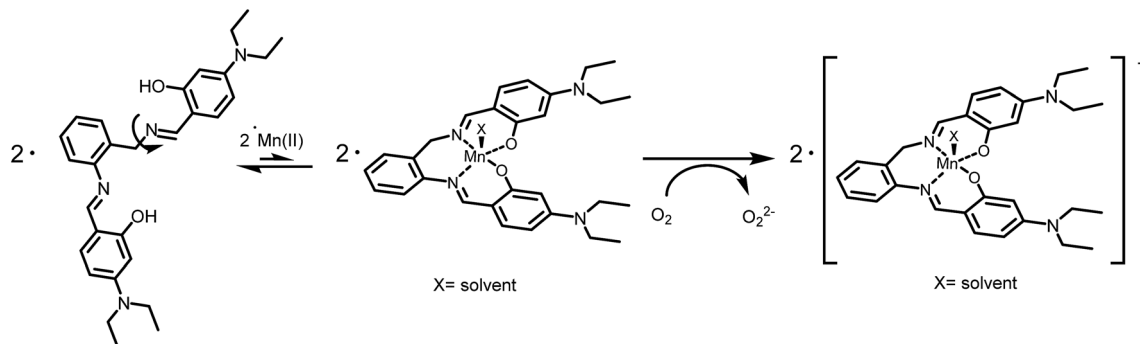**Fig. 11** Color changes of **1** (10 μM) 4 h after 1.3 equiv. of Mn²⁺ and Mn³⁺ ions were added into **1**, respectively, in 10 mM bis-tris buffer/CH₃CN (7 : 3, v/v) under the degassed conditions.

Scheme 3 Proposed sensing mechanism of Mn^{2+} by **1**.

demonstrate that **1** does not detect Mn^{2+}, but Mn^{3+} through color change from pale yellow to reddish brown.

To more clearly confirm our proof of the oxidation of Mn^{2+} to Mn^{3+} in the **1**–Mn^{2+} complex, we used electron paramagnetic resonance (EPR) spectroscopy (Fig. 12). As expected, **1**–Mn^{3+} samples prepared under aerobic conditions showed typical silent signals suggestive to Mn^{3+} regardless of the reaction time (10 m through 4 h, Fig. 12a). **1**–Mn^{2+} samples prepared under aerobic conditions showed typical signals at $g = 2.03$ and 2.04 suggestive to Mn^{2+}. However, the EPR signals of the **1**–Mn^{2+} samples gradually decreased and disappeared after 4 h (Fig. 12b). These results confirm that **1**–Mn^{2+} complexes formed from the reaction of **1** with Mn^{2+} ions were gradually oxidized to **1**–Mn^{3+} complexes by oxygen molecules over 4 h. Based on Job plot, the degassed experiment, EPR study, and ESI-mass spectrometry analysis, we propose the reaction mechanism for the formation of **1**–Mn^{3+} complex produced from the reaction of **1** with Mn^{2+} ion as shown in Scheme 3. We assume that **1**–Mn^{2+} complex exists in a small ratio by an easy rotation of the benzyl carbon of **1** at equilibrium (the first step in Scheme 3), because Mn^{2+} ion with lower oxidation state may not strongly bind to two oxygen atoms of **1**. In contrast, Mn^{3+} ion with higher oxidation state may form **1**–Mn^{3+} complex easily. Therefore, the small portion of **1**–Mn^{2+} complex under aerobic condition would be oxidized slowly to **1**–Mn^{3+} complex by O_2. In comparison, a similar type of chemosensor (**L**, 9th row in Table 1), which do not contain a benzyl carbon,[38] seems to react quickly with Mn^{2+} to form **L**–Mn^{2+} complex, thus resulting in quick sensing of Mn^{2+}.

The binding constant of **1** with Mn^{2+} was calculated as 2.0×10^4 M^{-1} on the basis of Benesi–Hildebrand equation (Fig. S8†),[43] which was nearly identical to that of the **1**–Mn^{3+} complex. This values is within those (10^3 to 10^{12}) previously reported for Mn^{2+}-binding chemosensors.[4,11,35,36,45] Based on the result of UV-vis titration, the detection limit for **1**–Mn^{2+} was determined to be 0.91 μM on the basis of the definition by IUPAC ($C_{DL} = 3S_b/m$, Fig. S9†), which is also nearly identical to that of the **1**–Mn^{3+} complex. Importantly, the value (0.91 μM) of **1** for Mn^{2+} is far below the World Health Organization (WHO) guideline (7.28 μM) of the drinking water,[46–48] suggesting that **1** could be an influential chemosensor for the detection of manganese in the drinking water.

3.4 Theoretical sensing mechanism

To obtain a deeper insight into the sensing mechanisms of **1** toward Mn^{3+}, theoretical calculations were performed in parallel to the experimental studies. As Job plot and ESI-mass spectrometry analysis showed that **1** reacted with Mn^{3+} in a 1 : 1 stoichiometric ratio, the theoretical calculations were performed with 1 : 1 stoichiometry. The exact coordination of **1** with Mn^{3+} could not be established since single crystal growth was not successful. However, the reported similar single crystal structures[46–48] and ESI-mass spectrometry analysis led us to propose that the **1**–Mn^{3+} complex might have square pyramidal coordination geometry with one solvent molecule (acetonitrile, see Scheme 2). Also, based on the EPR spectroscopy, **1**–Mn^{3+} complex was optimized with a paramagnetic complex ($S = 3$, DFT/uB3LYP/main group atom: 6-311+G** and Mn: Lanl2DZ/ECP). The significant structural properties of the energy-minimized structures are shown in Fig. S10.†

We also investigated the absorption to the singlet excited states of **1** and **1**–Mn^{3+} complex via TDDFT calculations. In case of **1**, the main molecular orbital (MO) contribution of the first lowest excited state was determined for HOMO → LUMO transition (362.50 nm, Table S1 and Fig. S11†), which indicated an intramolecular charge transfer (ICT) band. In case of **1**–Mn^{3+} complex, the excited states of 10th, 22nd and 30th (552.33, 410.69 and 378.60 nm) were found to be relevant for the observed color change (yellow to reddish brown) showing the predominance of LMCT and ICT (Table S2 and Fig. S12 and S13†). These results were well consistent with the experimental absorption wavelengths. Thus, the chelation of Mn^{3+} with **1** mainly showed the LMCT and ICT, which induced the color change of **1** in the presence of Mn^{3+}.

4. Conclusions

We have developed a selective and efficient Schiff base chemosensor for the simultaneous detection of Mn^{2+} and Mn^{3+}. The sensor **1** exhibited an excellent selectivity toward Mn^{2+} and Mn^{3+} over competing relevant metal ions in aqueous media. Additionally, this sensor **1** can discriminate Mn^{3+} from Mn^{2+}, based on their time-dependent color changes according to the reaction time. In addition, the detection limits (0.91 and 0.64 μM) of **1** for both Mn^{2+} and Mn^{3+} were far below the guideline of

the WHO (7.28 μM). Additionally, sensor **1** could be recycled simply through treatment with a proper reagent such as EDTA, and can be used to detect and quantify Mn^{3+} in water samples. Moreover, the colorimetric detection of Mn^{3+} by using the test strip coated with **1** was successfully achieved. Furthermore, the sensing mechanism of Mn^{3+} was explained by theoretical calculations. Therefore, we believe that this Schiff based sensor could be an important guidance to the development of a new type of the colorimetric chemosensors for the simultaneous detection of Mn^{2+} and Mn^{3+}.

Acknowledgements

References

1 A. P. de Silva, H. Q. N. Gunaratne, T. Gunnlaugsson, A. J. M. Huxley, C. P. McCoy, J. T. Rademacher and E. Rice, *Chem. Rev.*, 1997, **97**, 1515–1566.

2 B. Valeur and I. Leray, *Coord. Chem. Rev.*, 2000, **205**, 3–40.

3 J. Y. Noh, S. Kim, I. H. Hwang, G. Y. Lee, J. Kang, S. H. Kim, J. Min, S. Park, C. Kim and J. Kim, *Dyes Pigm.*, 2013, **99**, 1016–1021.

4 İ. Kaya, M. Yıldırım and M. Kamacı, *Synth. Met.*, 2011, **161**, 2036–2040.

5 S. A. Lee, G. R. You, Y. W. Choi, H. Y. Jo, A. R. Kim, I. Noh, S. Kim, Y. Kim and C. Kim, *Dalton Trans.*, 2014, **43**, 6650–6659.

6 G. R. You, G. J. Park, S. A. Lee, Y. W. Choi, Y. S. Kim, J. J. Lee and C. Kim, *Sens. Actuators, B*, 2014, **202**, 645–655.

7 G. J. Park, H. Y. Jo, K. Y. Ryu and C. Kim, *RSC Adv.*, 2014, **4**, 63882–63890.

8 W. Liu, J. Jiang, C. Chen, X. Tang, J. Shi, P. Zhang, K. Zhang, Z. Li, W. Dou, L. Yang and W. Liu, *Inorg. Chem.*, 2014, **53**, 12590–12594.

9 J. Li, J. Gao, W.-W. Xiong, P.-Z. Li, Q. Zhang, Y. Zhao and Q. Zhang, *Chem.–Asian J.*, 2014, **9**, 121–125.

10 Y. J. Na, G. J. Park, H. Y. Jo, S. A. Lee and C. Kim, *New J. Chem.*, 2014, **38**, 5769–5776.

11 S. Xu, C. Wang, H. Zhang, Q. Sun, Z. Wang and Y. Cui, *J. Mater. Chem.*, 2012, **22**, 9216–9221.

12 D. B. Calne, N.-S. Chu, C.-C. Huang, C.-S. Lu and W. Olanow, *Neurology*, 1994, **44**, 1582–1596.

13 A. Takeda, *Brain Res. Rev.*, 2003, **41**, 79–87.

14 K. L. Mutaftchiev, *Anal. Lett.*, 2004, **37**, 2869–2879.

15 G. Oszlanczi, T. Vezer, L. Sarkozi, E. Horvath, Z. Konya and A. Papp, *Ecotoxicol. Environ. Saf.*, 2010, **73**, 2004–2009.

16 N. Hayakawa, S. Asayama, Y. Noda, T. Shimizu and H. Kawakami, *Mol. Pharmaceutics*, 2012, **9**, 2956–2959.

17 B. Michalke and K. Fernsebner, *J. Trace Elem. Med. Biol.*, 2014, **28**, 106–116.

18 J. Jankovic, *J. Neurol.*, 2005, **64**, 2021–2028.

19 Z.-R. Tian, W. Tong, J.-Y. Wang, N.-G. Duan, V. V. Krishnan and S. L. Suib, *Science*, 1997, **276**, 926–930.

20 P. A. Loach and M. Calvin, *Biochemistry*, 1963, **2**, 361–371.

21 J.-Y. Chen, G. C. Tsao, Q. Zhao and W. Zheng, *Toxicol. Appl. Pharmacol.*, 2001, **175**, 160–168.

22 Z. Dai, N. Khosla and J. W. Canary, *Supramol. Chem.*, 2009, **21**, 296–300.

23 Y. J. Lee, C. Lim, H. Suh, E. J. Song and C. Kim, *Sens. Actuators, B*, 2014, **201**, 535–544.

24 K. B. Kim, G. J. Park, H. Kim, E. J. Song, J. M. Bae and C. Kim, *Inorg. Chem. Commun.*, 2014, **46**, 237–240.

25 A. D. Becke, *J. Chem. Phys.*, 1993, **98**, 5648–5652.

26 C. Lee, W. Yang and R. G. Parr, *Phys. Rev. B: Condens. Matter Mater. Phys.*, 1988, **37**, 785–789.

27 M. J. Frisch, G. W. Trucks, H. B. Schlegel, G. E. Scuseria, M. A. Robb and J. R. Cheeseman, *et al.*, *Gaussian 03, revision D.01*, Gaussian, Inc, Wallingford CT, 2004.

28 P. J. Hay and W. R. Wadt, *J. Chem. Phys.*, 1985, **82**, 270–283.

29 P. J. Hay and W. R. Wadt, *J. Chem. Phys.*, 1985, **82**, 284–298.

30 P. J. Hay and W. R. Wadt, *J. Chem. Phys.*, 1985, **82**, 299–310.

31 V. Barone and M. Cossi, *J. Phys. Chem. A*, 1998, **102**, 1995–2001.

32 M. Cossi and V. Barone, *J. Chem. Phys.*, 2001, **115**, 4708–4717.

33 N. M. O'Boyle, A. L. Tenderholt and K. M. Langner, *J. Comput. Chem.*, 2008, **29**, 839–845.

34 J. Liang and J. W. Canary, *Angew. Chem., Int. Ed.*, 2010, **49**, 7710–7713.

35 F. Gruppi, J. Liang, B. B. Bartelle, M. Royzen, D. H. Turnbull and W. Canary, *Chem. Commun.*, 2012, **48**, 10778–10780.

36 C. Gou, H. Wu, S. Jiang, C. Yi, J. Luo and X. Li, *Chem. Lett.*, 2011, **40**, 1082–1084.

37 K. Dutta, R. C. Deka and D. K. Das, *J. Fluoresc.*, 2013, **23**, 1173–1178.

38 P. S. Hariharan and S. P. Anthony, *Spectrochim. Acta, Part A*, 2015, **136**, 1658–1665.

39 H. Asada, M. Ozeki, M. Fujiwara and T. Matsushita, *Polyhedron*, 2002, **21**, 1139–1148.

40 T. Gupta, M. K. Saha, S. Sen, S. Mitra, A. J. Edwards and W. Clegg, *Polyhedron*, 1999, **18**, 197–201.

41 A. Panja, N. Shaikh, S. Gupta, R. J. Butcher and P. Banerjee, *Eur. J. Inorg. Chem.*, 2003, 1540–1547.

42 P. Job, *Ann. Chim.*, 1928, **9**, 113–203.

43 H. A. Benesi and J. H. Hildebrand, *J. Am. Chem. Soc.*, 1949, **71**, 2703–2707.

44 K. Ljung and M. Vahter, *Environ. Health Perspect.*, 2007, **115**, 1533–1538.

45 X. Mao, H. Su, D. Tian, H. Li and R. Yang, *ACS Appl. Mater. Interfaces*, 2013, **5**, 592–597.

46 E. N. Jacobsen, A. Pfaltz and H. Yamamoto, *Comprehensive Asymmetric Catalysis*, Springer, Berlin, 1999, pp. 649–677.

47 M. Suzuki, T. Ishikawa, A. Harada, S. Ohba, M. Sakamoto and Y. Nishida, *Polyhedron*, 1997, **16**, 2553–2561.

48 P. S. Hariharan and S. P. Anthony, *Anal. Chim. Acta*, 2014, **848**, 74–79.